Supplementary Material

1 SUPPLEMENTARY FIGURES

1.1 Figures

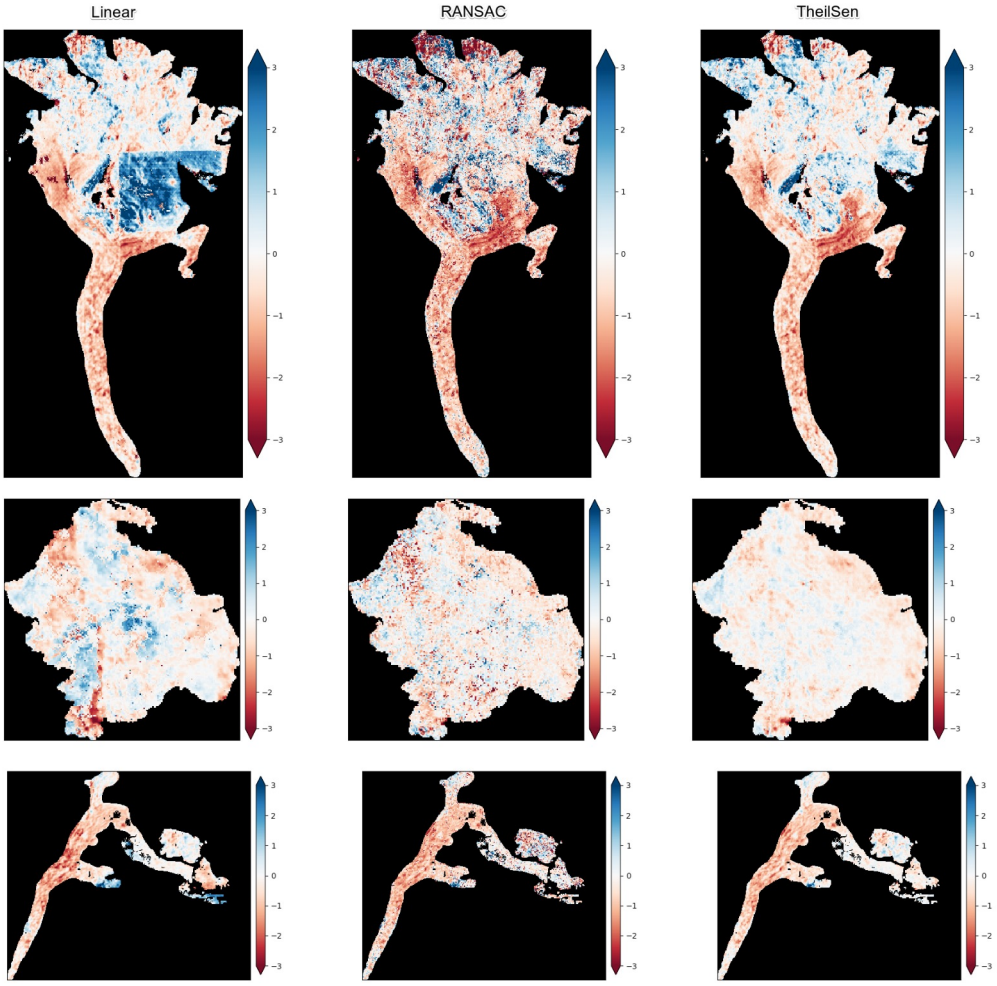

Figure S1. Comparison of different methods to compute elevation trend ($\frac{dh}{dt}$). Columns show linear regression, RANSAC, and Theil-Sen approaches for three sample glaciers (rows: Ngozumpa, RGI 13.00175, and Khumbu). Values are per-pixel elevation change rate in meters per year.

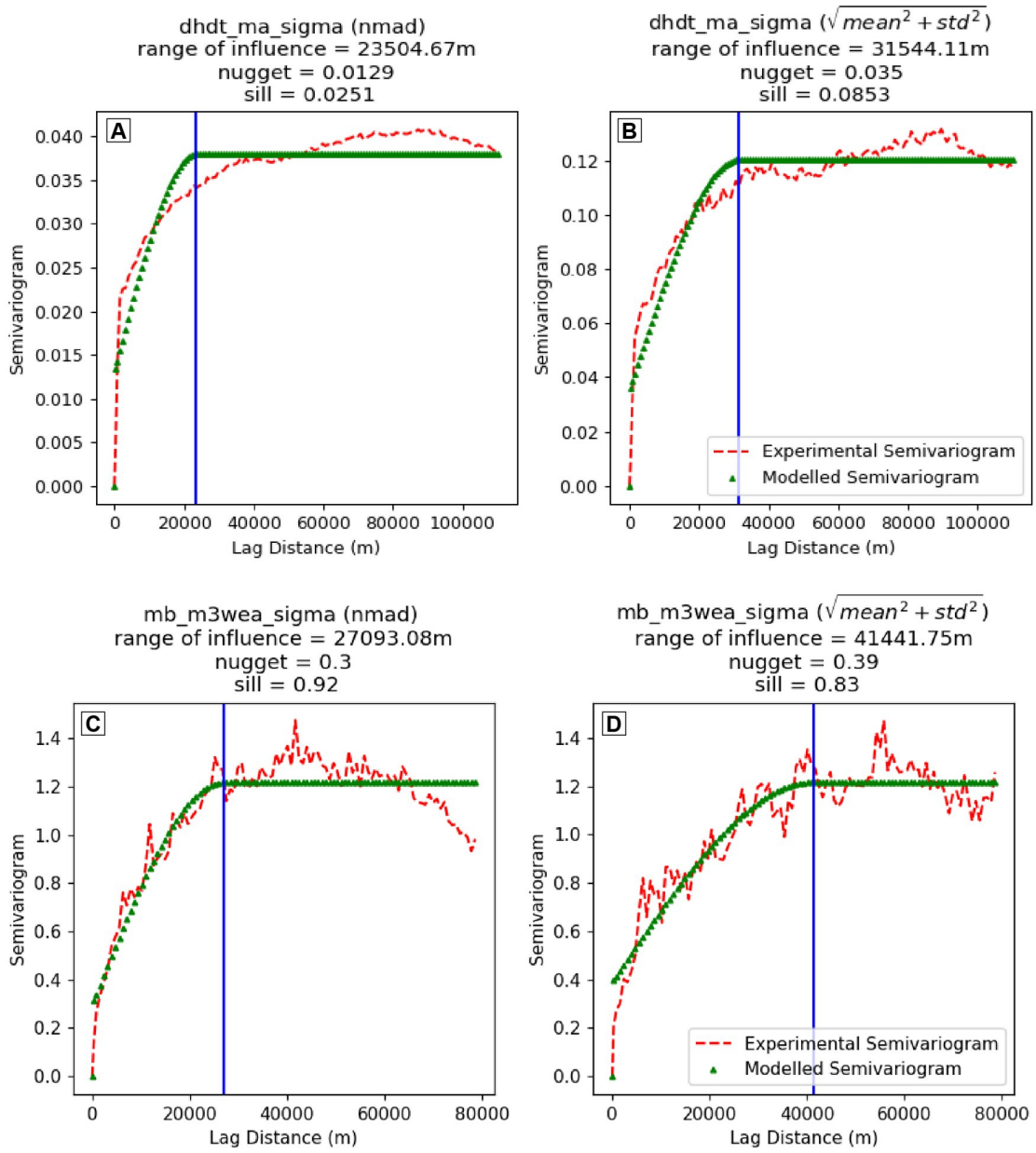

Figure S2. Spherical variogram fits used to assess spatial autocorrelation of glacier mass balance uncertainty values between glacier polygon centroids. Two different glacier mass balance uncertainty metrics were considered, using statistics for observed $\frac{dh}{dt}$ values over static surfaces around each polygon: A+C) NMAD, and B+D) RMSE ($\sqrt{mean^2 + std^2}$). Semivariograms were fit to $\sigma_{\Delta h}$ (A+B) and combined $\sigma_{\Delta M}$ (C+D) uncertainty. The red curve is the experimental semivariogram, the green curve is the corresponding modeled spherical semivariogram, and the blue line is the lag distance (range of influence) at which the model attains the sill value. See the processing notebooks `Mass_balance_cor_working.ipynb` and `dh_dt_sigma_error.ipynb` in the `raster_geostatistics` repository (Bhushan, 2019) for additional details.

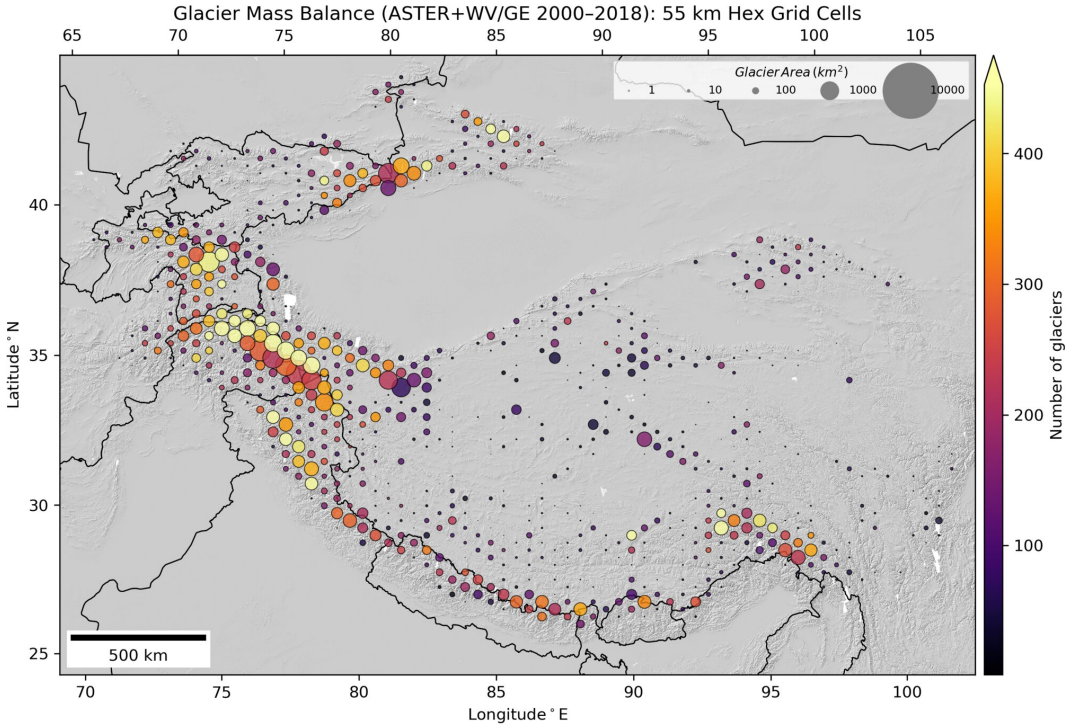

Figure S3. Count of glaciers with valid mass balance estimate in each 55-km hex cell. The size of the circle for each cell is scaled by total glacierized area within that cell. Approximate international borders from Natural Earth 1:10M products are plotted for reference.

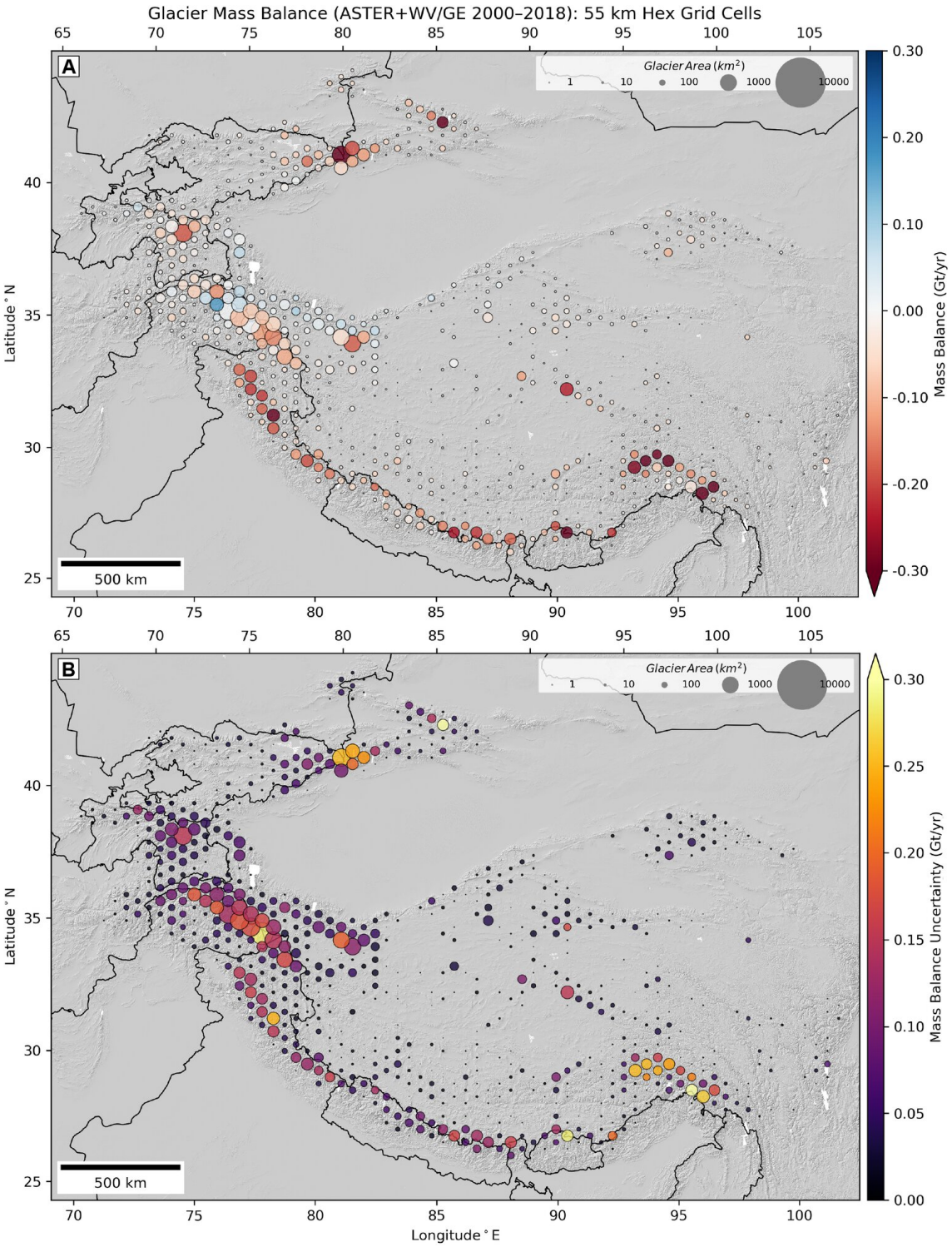

Figure S4. A) Total glacier mass balance (Gt yr^{-1}) and B) uncertainty estimates for 55-km hex cells. The size of the circle for each cell is scaled by total glacierized area within that cell. Approximate international borders from Natural Earth 1:10M products are plotted for reference.

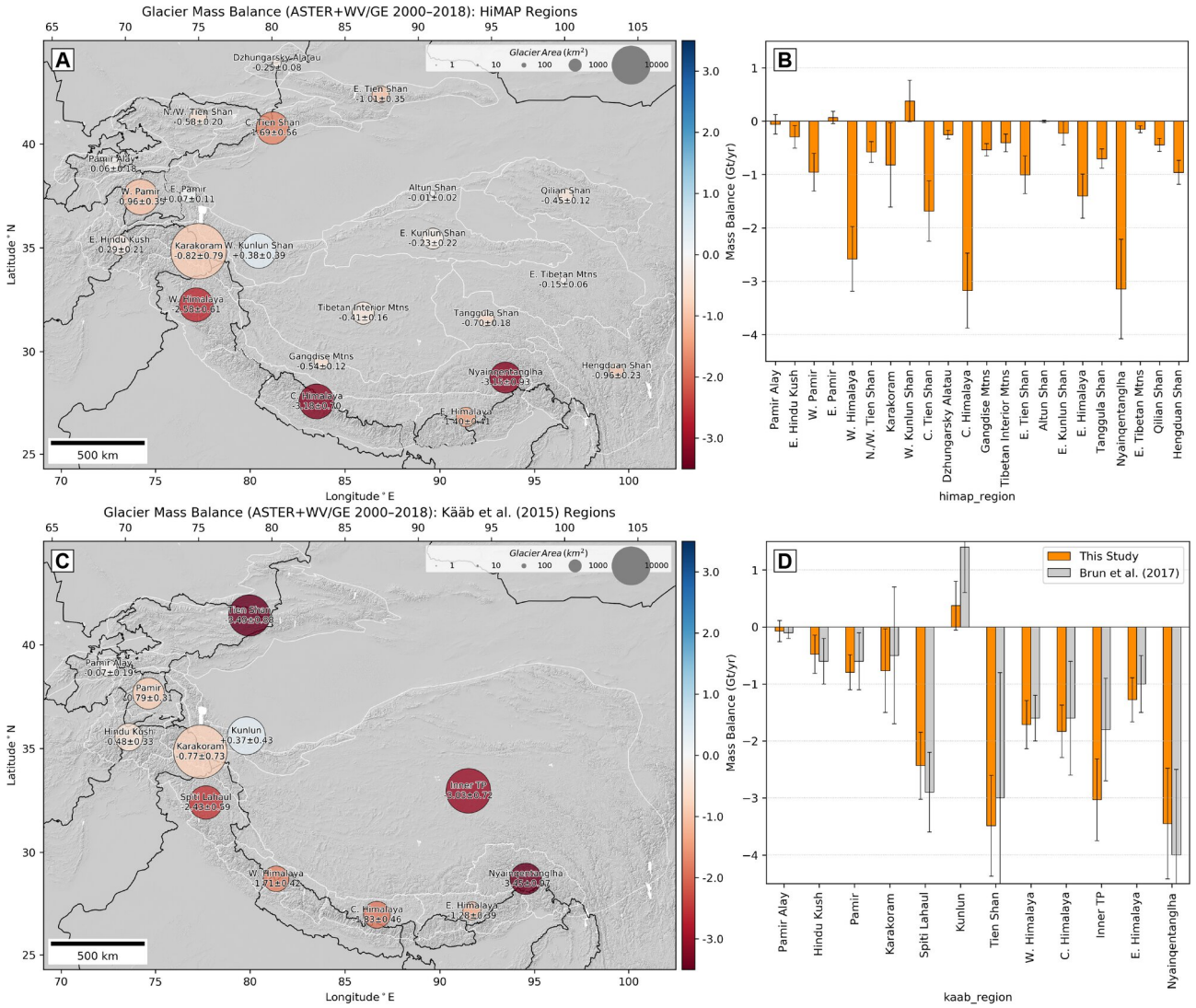

Figure S5. Aggregated total glacier mass balance (Gt yr^{-1}) for A-B) HiMAP regions (Bolch et al., 2019), and C-D) Kääb et al. (2015) regions. Circle color shows mass balance and circle size is scaled by total glacier area for each region (white outlines). Bar plots are sorted by x-coordinate of region centroid. Revised values (Brun et al., 2018) from Brun et al. (2017) are plotted in D for comparison.

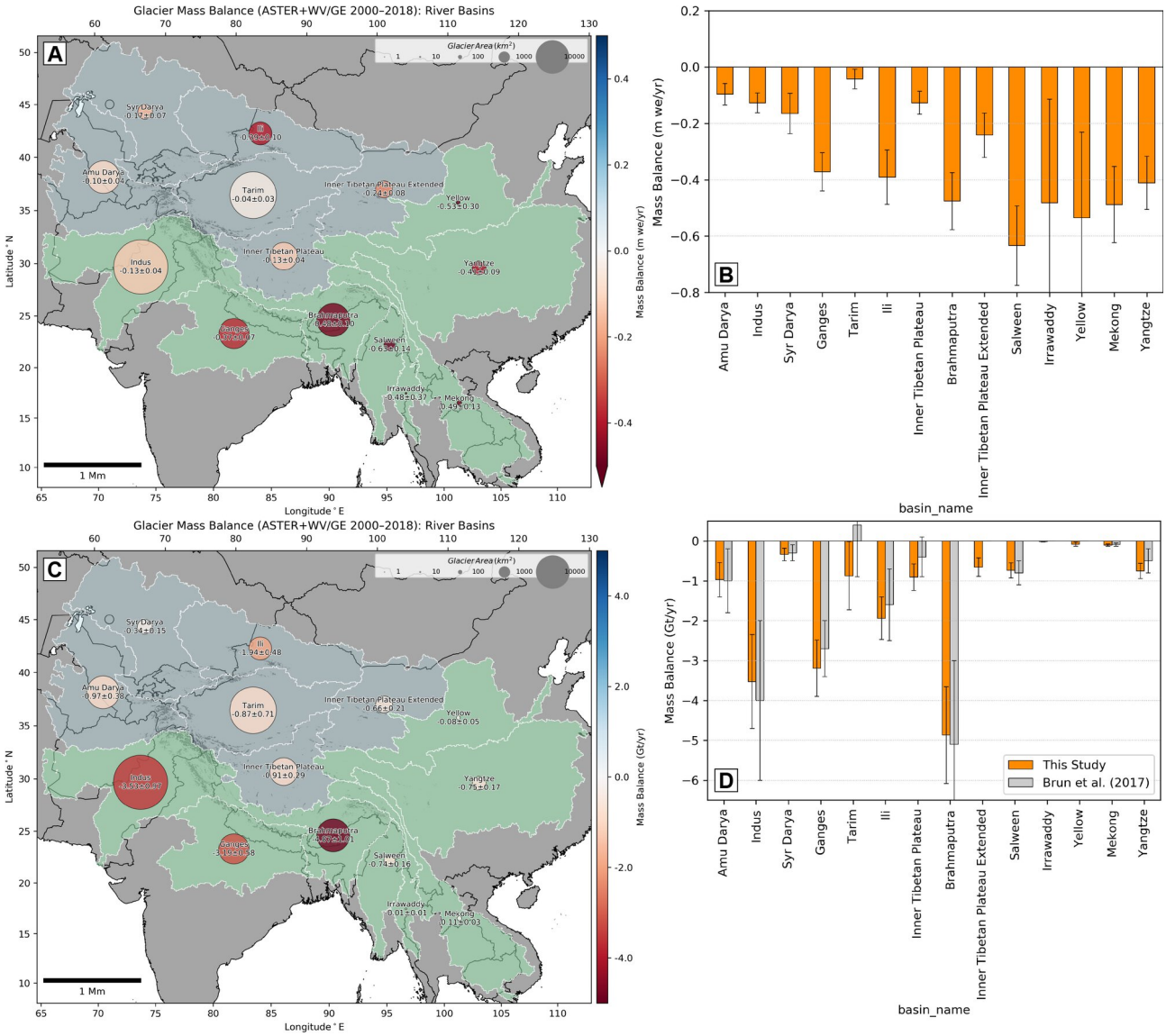

Figure S6. Aggregated specific glacier mass balance in m w.e. yr^{-1} (A+B) and total glacier mass balance in Gt yr^{-1} (C+D) for HMA river basins. Circle color shows mass balance and circle size is scaled by total glacier area in each basin (white outlines, with endorheic basins shaded blue, and exorheic basins shaded green). Bar plots are sorted by x-coordinate of basin centroid. Values from Brun et al. (2017) are plotted for comparison (not available for Inner Tibetan Plateau Extended, Irrawaddy, and Yellow).

REFERENCES

[Dataset] Bhushan, S. (2019). ShashankBice/raster_geostatistics: Updated code before manuscript submission. doi:10.5281/zenodo.3539726

Bolch, T., Shea, J. M., Liu, S., Azam, F. M., Gao, Y., Gruber, S., et al. (2019). Status and change of the cryosphere in the extended hindu kush himalaya region. In *The Hindu Kush Himalaya Assessment: Mountains, Climate Change, Sustainability and People*, eds. P. Wester, A. Mishra, A. Mukherji, and A. B. Shrestha (Cham: Springer). 209–255. doi:10.1007/978-3-319-92288-1_7

Brun, F., Berthier, E., Wagnon, P., Kääb, A., and Treichler, D. (2017). A spatially resolved estimate of high mountain asia glacier mass balances from 2000 to 2016. *Nat. Geosci.* 10, 668–673. doi:10.1038/ngeo2999

Brun, F., Berthier, E., Wagnon, P., Kääb, A., and Treichler, D. (2018). Author correction: A spatially resolved estimate of high mountain asia glacier mass balances from 2000 to 2016. *Nature Geoscience* 11, 543–543. doi:10.1038/s41561-018-0171-z

Kääb, A., Treichler, D., Nuth, C., and Berthier, E. (2015). Brief communication: Contending estimates of 2003–2008 glacier mass balance over the Pamir–Karakoram–Himalaya. *The Cryosphere* 9, 557–564. doi:10.5194/tc-9-557-2015